


Performance Analysis of Artificial Intelligence Controller for PV and Battery Connected UPQC

Koganti Srilakshmi * , S. Poorna Chander Rao ** , G. Deepika *** , B.V. Sai Thrinath **** ,
Alapati Ramadevi ***** , Sravanthy Gadameddi * , Kongari Dushanth Kumar * , Aravindhababu
Palanivelu ***** 

* Department of Electrical and Electronics Engineering, Sreenidhi Institute of Science and Technology, Hyderabad, India

** Department of Electrical and Electronics Engineering, Geethanjali College of Engineering and Technology, Hyderabad, India.

***Department of Electronics and Communication Engineering, St. Peters Engineering College, Hyderabad, India

**** Department of Electrical and Electronics Engineering, Mohan Babu University, Tirupathi, India

***** Department of Electrical and Electronics Engineering, Velagapudi Ramakrishna Siddhartha Engineering College, Kanuru, Vijayawada, Andhra Pradesh, India

***** Department of Electrical Engineering, Annamalai University, Chidambaram, India

(kogantisrilakshmi29@gmail.com, spoorna.eee@gcet.edu.in, gdeepika@stpetershyd.com, connectbvst@gmail.com, gaddipatiramadevi@gmail.com, sravanthi314@gmail.com, dushanthkumarkongari54@gmail.com, aravindhababu@gmail.com)

‡

Corresponding Author: Koganti Srilakshmi, Sreenidhi Institute of Science and Technology, Tel: +91-8885851666, kogantisrilakshmi29@gmail.com.

Received: 11.10.2022 Accepted: 20.11.2022

Abstract: Nowadays, integration of the non-conventional energy sources like wind, tidal, solar etc into the grid is suggested in order to minimize the losses in the distribution network and to meet the demand. The arrival of the power electronics equipments to control the nonlinear loads has made an impact on the power quality. The unified power quality conditioner (UPQC) is a FACTS device with the back to back converters, coupled together with a DC-Link capacitor. This paper suggests an intelligent hybrid controller for the solar Photo-voltaic system and Battery storage system integrated UPQC. The proposed controller adapts both the qualities of artificial neural network and Integral sliding-mode controller. The synchronization of phases is created by self tuning filter (STF) in association with unit vector generation method (STF-UVGM) for the superior performance of UPQC during the unbalanced/ distorted supply voltages conditions. Therefore, the necessity of Phase-locked-loop, Low pass filters and High pass filters are eliminated. However, STF is used for separating the Harmonic and Fundamental components. In addition, STF-UVGM was used for generation of synchronization phases of series and shunt filters. The prime objectives of the suggested artificial neural network integral sliding mode hybrid controller (ANNISMHC) are fast action to retain the DC-Link voltage to the constant value during load/ irradiation variations, diminish the harmonics in the current waveforms, power-factor enhancement, maximum mitigation of sag, swell and disturbances in supply voltage, and compensation for the unbalanced supply voltages. The working of suggested ANNISMHC was investigated on five test cases for several combinations of loads, and balanced/unbalanced supply voltages. However, to demonstrate supremacy of the suggested ANNISMHC comparative study with the different controllers those are available in literature and also with the standard controllers like PIC, SMC, and FLC. The ANNISMHC shows an extra-ordinary performance in diminishing THD thereby improving PF and reducing voltage distortions.

Keywords- Self tuning filter, Fuzzy-Logic controller, Unified Power Quality Conditioner, Solar PV generation, Battery system

Nomenclature:		$V_{s_{-\alpha}}, V_{s_{-\beta}}, V_{s_{-0}}$	FC of source voltage in $\alpha - \beta - 0$ frame
SUAPF	Shunt active power filter	R_s	Supply Resistance
SEAPF	Series active power filter	L_s	Supply Inductance
PQ	Power Quality		
UPQC	Unified Power Quality Conditioner	$V_{l_{-a}}, V_{l_{-b}}, V_{l_{-c}}$	Load voltages in abc phases
SPV	Solar Photo-Voltaic	$V_{se_{-a}}, V_{se_{-b}}, V_{se_{-c}}$	Compensated series voltage in abc frame
BS	Battery Storage	$V^{ref}_{-a}, V^{ref}_{-b}, V^{ref}_{-c}$	Reference-voltages in abc
FLC	Fuzzy Logic Controller		
ANNC	Artificial neural network controller	$V^{ref}_{se_{-d}}, V^{ref}_{se_{-q}}$	Series injected reference voltage in $d - q$ frame
PIC	Proportional Integral Controller	$V^{ref}_{se_{-\alpha}}, V^{ref}_{se_{-\beta}}$	Series injected reference voltage in $\alpha - \beta$ frame
SMC	Sliding-mode Control	$V^{ref}_{-\alpha}, V^{ref}_{-\beta}$	Reference-voltage in $\alpha - \beta$ frame
ISMC	Integral Sliding-mode Control		
SYP	Synchronization Of Phases	$V^{ref}_{-d}, V^{ref}_{-q}$	Reference-voltage in $d - q$ frame
STF	Self Tuning Filter		
SMC	Sliding mode control	$i_{l_{-a}}, i_{l_{-b}}, i_{l_{-c}}$	Load current in abc frame
UVGM	Unit Vector Generation Method	$i_{l_{-\alpha}}, i_{l_{-\beta}}, i_{l_{-0}}$	Load currents in $\alpha - \beta - 0$ frame
PLL	Phased locked Loop	$\dot{i}_{l_{-\alpha}}, \dot{i}_{l_{-\beta}}, \dot{i}_{l_{-0}}$	FC of load current in $\alpha - \beta - 0$ frame
LPFs	Low pass Filters		
HPFs	High Pass Filters	$\ddot{i}_{l_{-\alpha}}, \ddot{i}_{l_{-\beta}}, \ddot{i}_{l_{-0}}$	HC of load current in $\alpha - \beta - 0$ frame
FC	Fundamental Component		
HC	Harmonic Component	$\ddot{i}_{l_{-d}}, \ddot{i}_{l_{-q}}$	HC of load current in $d - q$ frame
HL	Hidden Layer		
IL	Input Layer	$i^{ref}_{l_{-a}}, i^{ref}_{l_{-b}}, i^{ref}_{l_{-c}}$	Reference load current in abc frame
OP	Output Layer		
MLP	Multi layer perceptron	$i^{ref}_{l_{-\alpha}}, i^{ref}_{l_{-\beta}}, i^{ref}_{l_{-0}}$	Reference load current $\alpha - \beta - 0$ frame
PF	Power Factor		
IOT	Internet of Things	$i^{ref}_{l_{-d}}, i^{ref}_{l_{-q}}$	Reference load current in $d - q$ frame
DSTATCOM	Distributed static compensator	$i_{sh_{-a}}, i_{sh_{-b}}, i_{sh_{-c}}$	SUAPF injected current for phases a, b, c
$V_{s_{-a}}, V_{s_{-b}}, V_{s_{-c}}$	Supply voltage for abc	$i^{ref}_{sh_{-a}}, i^{ref}_{sh_{-b}}, i^{ref}_{sh_{-c}}$	Reference SUAPF injected current for phases abc
$i_{s_{-a}}, i_{s_{-b}}, i_{s_{-c}}$	Supply current for abc	$i_{sh_{-a}}, i_{sh_{-b}}, i_{sh_{-c}}$	SUAPF injected current for abc phases
$V_{s_{-\alpha}}, V_{s_{-\beta}}, V_{s_{-0}}$	Supply voltage in $\alpha - \beta - 0$ frame		

C_{sh}	SUAPF Capacitance
R_{sh}	Capacitance of SUAPF
L_{sh}	Resistance of SUAPF
C_{dc}	Inductance of SUAPF
V_{dc}	Capacitance at DC link
V_{dc}^{ref}	Reference voltage at DC link
i_{dc}^{ref}	Reference current at DC link
Δi_{dc}	output current error of DC-Link
P_{PV}	Power output of PV system
V_{PV}	Voltage output of PV system
I_{PV}	Current output of PV system
$P_{DC-Link}$	DC link power
P_{BS}	Power output of battery-system
V_{BS}	Voltage of battery-system
i_{BS}	Current of battery-system
Q	Capacity of battery
DPD	DC-Link power demand
SRFT	Synchronous Reference-Frame Theory
BC	Boost-Converter
BBC	Buck Boost Converter
$SOCB$	State of charge of the Battery
SPG	Solar output Power Generated

1. Introduction

Nowadays, power distribution system is facing PQ related problems like interruptions, disturbances, flicker, sag/swell, and harmonics, PF etc due to the integration of inconsistent behavior wind, tidal, solar etc, the large non linear and unbalanced loads with power electronic equipments. However, this increased usage of the large non-linear industrial-loads leads to the decline in PF. Therefore, maintain of PQ has become the primary challenge to the power Engineers. The various configurations of single and /three phase SUAPF with various control techniques was suggested for three and four wire distribution systems for balanced and unbalanced supply voltages circumstances to

attend PQ issues. In addition, the most recent developments and applications of SUAPF were also discussed [1]. The novel controller based on SRFT was designed for the 3 ϕ -4wire UPQC to eliminate PQ related problems effectively for both the un-balanced/ distorted loads of distribution system [2].

A hybrid controller with the combination of both FL and PI properties was developed for SUAPF with an aim of reducing THD to within the standards. To show the superiority of the proposed controller case study analysis was done for balanced and/ unbalanced loads [3]. Besides, the STF based solar battery connected SUAPF was developed in view of regulating the reactive power and minimizing current harmonics efficiently. While, to generate appropriate reference current the Maximal filter was introduced [4]. Further, the improvement in the intelligent based controllers like FL, ANN etc for SUAPF were able to addresses PQ problems effectively even for the dynamic load changes [5-7].

The PV associated UPQC was designed and ability was tested on different load variations through the maximum power tracking with an aim of diminishing THD and boosting the overall performance of UPQC [8]. Besides, the SRFT based PI controller was designed for the fuel cell supported SUAPF with a goal of suppressing the current harmonics effectively and to regulate the voltage across DC-Link [9]. Soccer league algorithm based optimal design of ANN controller was proposed to solar battery integrated UPQC to address power quality issues of distribution network [10]. However, to regulate the voltage and to control the reactive power at the grid a feed forward training based ANN controller was implemented on wind/solar associated UPQC [11].

A soccer league algorithm based optimal tuning of PI controller for UPQC was proposed to address the voltage and current PQ issues effectively [12]. Besides, a multilevel UPQC associated with the PV/ wind and fuel cell was projected with an aim of eliminating voltage distortions and current harmonics efficiently [13]. The UPQC was recommended in order to suppress the current/ voltage harmonics for furnace load at steel power plant. However, to prove its superior performance comparative analysis was carried out with DSATCOM [14]. The development of efficient controller through the combination of properties of both ANN, FL was carried out for the solar PV integrated UPQC to address the PQ problems and to show the viability of the proposed controller performance investigation was carried out for several combinations of the loads as well as supply voltages [15]. P-Q theory based control technique was suggested for UPQC using a STF and eliminating usage of LPFs or PLL [16].

The STF based SUAPF was designed to eliminate the requirement of LPF and/ PLL and to reduce THD. However, to prove its viability theoretical and/ practical performance investigation was done [17]. The UPQC with FL controller was suggested for non-linear R-L loads in order to suppress current harmonics thereby reducing the waveform imperfections [18]. A new Predictive phase dispersion method was suggested for the Multi-Level UPQC with a

main aim of reducing source voltage fluctuations, load current harmonics, and maintaining stable voltage at DC-Link [19]. The Fourier-Transform was recommended for solar/ Wind/ Fuel-cell, and Battery connected UPQC with an aim of eliminating voltage distortions in the supply voltage and reducing imperfections in load current [20]. The neuro-fuzzy based hybrid controller was recommended for UPQC to suppress the current harmonics and DC-Link balancing in distribution network for different loading conditions [21].

The SOL based load flow (LF) for both transmission and distribution systems was presented with a objective of minimizing the sum of the squares of the active, and reactive power mismatches at all the busses, while considering the net deviations of bus voltage angles, and magnitudes as unknown variables [22]. The intelligent Fuzzy-PI, Fuzzy-PID controllers was suggested to the AC-DC microgrid with a target of addressing PQ problems and thereby enhancing the voltage stability. Moreover, the performance was demonstrated on two test cases with variable loads [23]. An Adaptive full-order based technique was suggested to UPQC for rapid response in fault identification with high accuracy for all dynamic loads changes and grid conditions. Additionally, a BBO metaheuristic algorithm was used for tune K_p / K_i of PI controller optimally to stabilize the DC-Link oscillations [24].

UPQC was employed to eliminate the voltage imbalances and to reduce imperfections in current harmonics by adaptive neuro-fuzzy hybrid controller in addition to the improvement in the utilization of network [25]. A novel automatic shifting between grid/ or island was designed for the solar-battery connected UPQC to reduce PQ issues, in addition validation was carried out with experimental results [26]. The FL controller was suggested for SEAPF for to attend the PQ issues like voltage imperfections, minimizing THD with regulating DC link capacitor voltage [27]. The benefits and challenges of integrating the renewable energy sources into the grid and their control strategies was studied [20]. The effects on the smart grid technologies on the national grid were highlighted and few suggestions were also given to convert conventional grid into smart grid [21]. The comparison between P & O and PSO algorithms to get MPP for the PV system was studied for solar irradiation changes [22]. Experimental set-up of isolated boost full bridge DC-DC converter was investigated along with a set of low loss active snubber circuit [23]. Integration of renewable sources to micro grid for MPPT was studies with power management [24]. High voltage isolated ACDC converters were developed based on the modular technology [25]. FDNE based method was developed based on online least square identification algorithm along with digital simulators [26]. Fuzzy logic controller was suggested for PV-MPPT to improve the overall performance by maximum power point tracking [27].

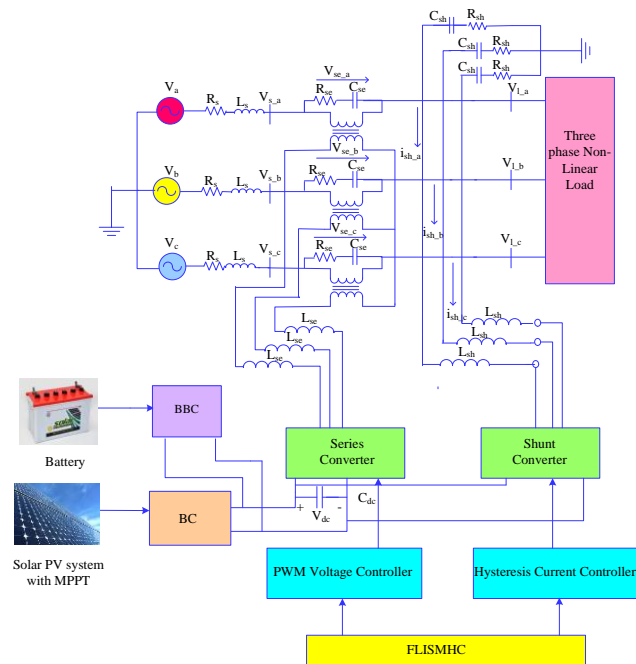


Fig.1. Components of U-SPBS

Although many of controllers were developed, still there exists a scope for developing a new hybrid controllers and intelligent techniques for efficiently handling the PQ related issues. In this paper, a hybrid controller with the combination of ANNC and ISMC properties was designed for UPQC connected to SPV and BS systems (U-SPBS) with the objective of diminishing the current THD thereby enhancing PF, regulating the voltage across the DC link during load/solar-irradiation variations, compensation during with voltage sag, swell and disturbance condition. The STF-UVGM was suggested to generate SYP for both SEAPF, and SUAPF instead of PLL. However, STF also eliminates LPFs and HPFs for separating the FC and HC of current. The performance analysis of the projected ANNISMHC for U-SPBS system was carried out for five different test cases, and to exhibit its supremacy comparative study was done with the conventional methods like PIC, SMC, FLC other controllers that exists in literature. Section2 gives the construction of U-SPBS, section3 provides the design of the proposed ANNISMHC, Section-4 presents discussion of results, and section-5 is the Conclusion.

2. Construction of Proposed U-SPBS

The configuration of the proposed U-SPBS is shown in Fig.1. The SPV and BS are connected to the DC link of UPQC via a BC, and BBC. This paper designs a artificial neural network based hybrid controller ANNISMHC to exploit both the unique properties of ANNC and PIC. The UPQC is the arrangement of both the series and shunt converters. The role of SEAPF is to mitigate voltage related distortions like sags/ swell/disturbance, supply voltage unbalances. Beside, the isolation between Series converter and the power line are provided through injecting transformers. In addition, it injects suitable V_{se} into the grid. Similarly, the main objective of SUAPF is to suppress the

harmonics in current waveform by injecting suitable i_{sh} and fast response to maintain the constant DC-link voltage across the capacitor. The 3ω balanced /unbalanced R-L loads, induction furnace load were considered in this work.

Table 1: Solar-PV Panel and Battery Ratings

Device	Parameters	Values
Solar-PV panel (SPR-215-WHT-U)	Output-power	214.92W
	Open circuit voltage	48.3V
	Short-circuit current	5.8A
	Maximum Voltage/current	39.80 V /5.40A
	No of PV cells connected in parallel	11
Li-ion battery	Rated Capacity	350 Ah
	Maximum capacity	450 Ah
	Normal-Voltage	650 V
	Full voltage	756 V

The SPV and BS supports externally to the DC link of UPQC through a BC, BBC in a aim of regulating constant DC link voltage during various load combinations, and reduces the converter ratings as illustrated in Fig. 2. The SPV and BS ratings considered in this work are listed in Table 1. The power distribution of U-SPBS at the DC link is specified by Eq. (1).

$$P_{PV} + P_{BS} - P_{DC-Link} = 0 \quad (1)$$

2.1 SPV System

The SPV system converts the solar irradiation into electrical energy. It consists of three parts PV panels connected in series/ parallel with the MPPT, and BC as given in Fig. 2. The amount of solar power generation (SPG) depends on the irradiation on PV panels. The integration of SPV system to the DC-Link reduces the voltage ratings, stress on converters and demand on utility. The MPPT controller (Perturb and observe) is implemented to extort highest productivity from the solar system. The output power P_{PV} is evaluated by Eq. (2)

$$P_{PV} = V_{PV} . I_{PV} \quad (2)$$

2.2 BS System

BS controller contains a lead-acid type of battery connected to BBC. It provides the stable voltage across the DC-Link as given in Fig. 2. $SOCB$ is calculated by Eq. (3).

$$SOCB = 100(1 + \int i_{BS} dtQ) \quad (3)$$

The amount of power generated by the SPV will decides the state of operation of a battery: charging or discharging

by satisfying the upper and lower constraints given by Eq. (4).

$$SOCB_{min} \leq SOCB \leq SOCB_{max} \quad (4)$$

The i_{dc}^{ref} is estimated by minimizing the error of DC link voltage $V_{dc,error}$ by a PI-controller specified in Eq. (5)-(6). The reference error current of the battery $i_{BS,error}^*$ is calculated by PI controller through a battery's error current $i_{BS,error}$. Where, $i_{BS,error}$ is obtained by the difference of i_{dc}^{ref} and reference battery's current i_{BS}^{ref} specified in Eq. (7) received from Eq. (8)-(9).

$$V_{dc,error}(t) = V_{dc}^{ref} - V_{dc} \quad (5)$$

$$i_{dc}^{ref} = K_{p1} V_{dc,error}(t) + K_{i1} \int_0^t V_{dc,error}(t) dt \quad (6)$$

$$i_{BS,error}(t) = i_{dc}^{ref} - i_{BS}^{ref} \quad (7)$$

$$i_{BS,error}^* = K_{p2} i_{BS,error}(t) + K_{i2} \int_0^t i_{BS,error}(t) dt \quad (8)$$

Where,

$$i_{BS}^{ref} = \left(\frac{1}{1 + T.S} \right) * i_{BS} \quad (9)$$

$K_{p1}=0.7$, $K_{i1}=10.1$, $K_{p2}=2.77$ and $K_{i2} = 11.17$ gains are taken arbitrarily. Table 2 provides the power distribution across the DC-link under various levels of SPG.

Table 2: Power-sharing at DC-link

Intensity of SPG	Action
$SPG > P_{dc}$	Excess SPG is utilized to charge Battery till it attains $SOCB_{max}$
$SPG = P_{dc}$	SPG alone will supply P_{dc} .
$SPG < P_{dc}$	The difference power is provided by Battery until it attains $SOCB_{min}$.
Nil SPG	Only BS supplies P_{dc} .

3. Control Strategy of U-SPBS using STF

During the fault or change in load, the voltage across capacitor of the DC-link varies. So, it is very important to make DC-Link voltage stable within a short duration of time. In d-q theory, first currents and voltages are transformed into the clark's reference. In general, the conventional UPQC mechanism consists of SUAPF, SEAPF

and PLL. In this proposed system STF-UVGM is used to generate SYP from the distorted supply voltages and also performs the role of PLL, HPFs and LPFs for separating the FC/ HC of currents. So, the suggested system contains of a STF, SUAPF and a SEAPF. The switching of series and shunt VSCs are carried out with the PWM voltage and PWM hysteresis current controllers with ANNISMHC. The major parts of the proposed controlling structure are given below:

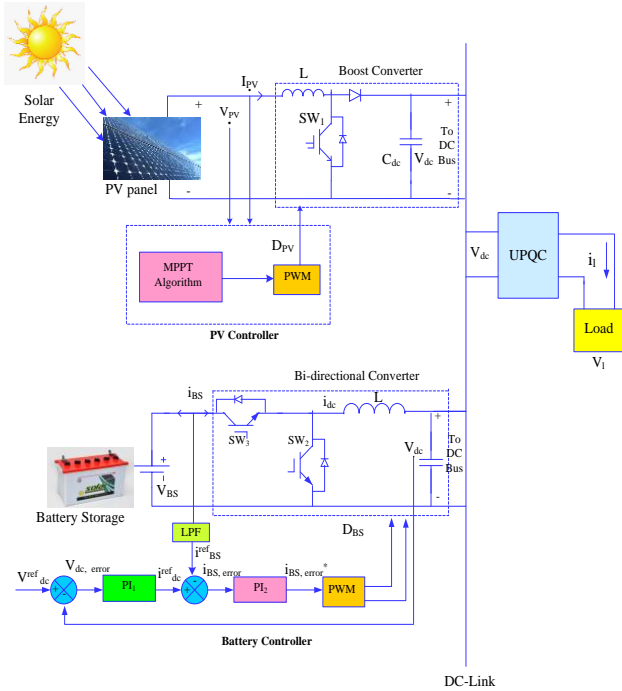


Fig.2. Proposed UPQC with PV and BS Controllers

3.1 STF-UVGM

The integral of SRFT was designed by Hong-Sock given in Eq. (10).

$$V_{xy}(t) = e^{j\omega t} \int e^{-j\omega t} U_{xy}(t) dt \quad (10)$$

Where, U_{xy} and V_{xy} are former and later integral signals in the SRF. The transfer-function $H(s)$ is provided in Eq.11 by implementing the Laplace transformation to Eq.10.

$$H(s) = \frac{V_{xy}(s)}{U_{xy}(s)} = \frac{s + j\omega}{s^2 + \omega^2} \quad (11)$$

To obtain STF a constant k has been established. Thus, $H(s)$ is as specified in Eq.12

$$H(s) = \frac{V_{xy}(s)}{U_{xy}(s)} = \frac{k(s+k) + j\omega_n}{(s+k)^2 + \omega_n^2} \quad (12)$$

By exchanging $U_{xy}(s)$ by $x_{\alpha\beta}(s)$ and $V_{xy}(s)$ by $x'_{\alpha\beta}(s)$, Eq. (13)-(14) is obtained:

$$x'_{\alpha} = \left(\frac{k}{s}\right)[x_{\alpha}(s) - x'_{\alpha}(s)] - \frac{\omega_n}{s} \cdot x'_{\beta}(s) \quad (13)$$

$$x'_{\beta} = \left(\frac{k}{s}\right)[x_{\beta}(s) - x'_{\beta}(s)] - \frac{\omega_n}{s} \cdot x'_{\alpha}(s) \quad (14)$$

Where, ω_n is the required frequency, and k is the gain.

If k decreases, the accuracy in obtaining the output decreases and vice-versa. Hence, by apply a STF control technique as shown in Fig.3 distorted voltage/ current signals can be obtained without any alter in magnitudes and phase angle.

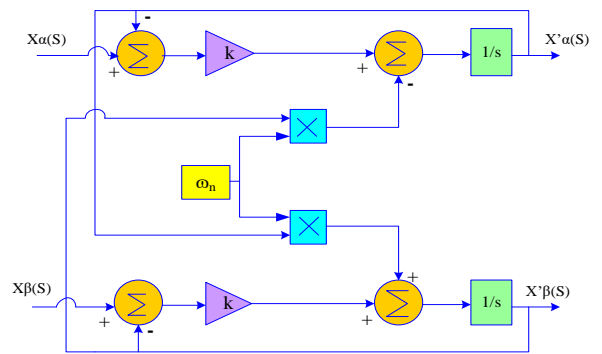


Fig.3. Controller of STF

3.2 STF-UVGM

The suggested STF-UVGM is non-iterative method which provides SYP from the supply voltage as shown in Fig. 4- 5. In Eq. 15 the Clarke's domain is used to transform the supply voltage from abc to $\alpha\beta 0$ domain.

$$\begin{bmatrix} V_{S-\alpha} \\ V_{S-\beta} \\ V_{S-0} \end{bmatrix} = \sqrt{\frac{2}{3}} \begin{bmatrix} 1 & -\frac{1}{2} & -\frac{1}{2} \\ 0 & \frac{\sqrt{3}}{2} & -\frac{\sqrt{3}}{2} \\ \frac{1}{2} & \frac{1}{2} & \frac{1}{2} \end{bmatrix} \begin{bmatrix} V_{S-a} \\ V_{S-b} \\ V_{S-c} \end{bmatrix} \quad (15)$$

The FC and HC are separated from the distorted grid voltages as given in Eq. 13 by considering only $\alpha\beta$ domain.

$$\begin{bmatrix} V_{S-\alpha} \\ V_{S-\beta} \end{bmatrix} = \begin{bmatrix} V'_{S-\alpha} + V''_{S-\alpha} \\ V'_{S-\beta} + V''_{S-\beta} \end{bmatrix} \quad (16)$$

Here, $V'_{S-\alpha}$ indicates the FC and $V''_{S-\alpha}$ indicates the HC in $\alpha\beta$ domain. The STF suppress the HC in the distorted grid voltages and extracts the FC to produce SYP with high quality. The Laplace transformation of STF is expressed by Eq. 17.

$$\begin{bmatrix} V'_{S-\alpha}(s) \\ V'_{S-\beta}(s) \end{bmatrix} = \frac{k1}{s} \begin{bmatrix} V_{S-\alpha}(s) - V'_{S-\alpha}(s) \\ V_{S-\beta}(s) + V'_{S-\beta}(s) \end{bmatrix} + \frac{2\pi f c1}{s} \begin{bmatrix} V'_{S-\beta}(s) \\ -V'_{S-\alpha}(s) \end{bmatrix} \quad (17)$$

Where, k_1 is the gain chosen as 20 and f_{c1} is the cut-off-frequency whose value is equal to the systems frequency 50Hz. The SYP $\sin(\omega t)$, $\cos(\omega t)$ are generated from Eq. 18 to omit PLL. STF-UVGM effectively generates SYP for distorted supply voltage of U-SPBS.

$$\begin{bmatrix} \sin(\omega t) \\ \cos(\omega t) \end{bmatrix} = \frac{1}{\sqrt{(V'_{s-\alpha})^2 + (V'_{s-\beta})^2}} \begin{bmatrix} V'_{s-\alpha} \\ -V'_{s-\beta} \end{bmatrix} \quad (18)$$

3.3 Shunt Controller

The main function of SUAPF is to suppress the current harmonics by injecting required amount of current, and to regulate DC capacitor voltage stable. The shunt-controller adapts (i) $abc - \alpha\beta$, $\alpha\beta - dq$, $dq - \alpha\beta$, and $\alpha\beta - abc$ transformations; (ii) proposed hybrid controller is applied for minimizing the THD and regulating the DC-link voltage. The controller compares the actual voltage of DC link with the reference voltage and transfers the current error output into the axis. The controller of the ANNISMHC is given in Fig. 4. The transformations of domains along with the STF, the design of ANNISMHC is given below:

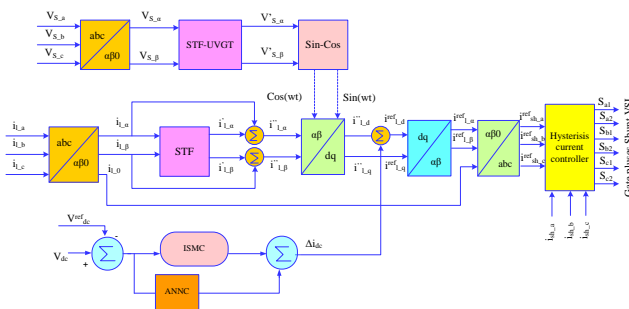


Fig.4. ANNISMHC for Shunt Converter

In SUAPF initially, the load currents are shifted to $\alpha - \beta - 0$ frames by applying clarke transformation adopting Eq.19.

$$\begin{bmatrix} i_{l-\alpha} \\ i_{l-\beta} \\ i_{l-0} \end{bmatrix} = \sqrt{\frac{2}{3}} \begin{bmatrix} 1 & -\frac{1}{2} & -\frac{1}{2} \\ 0 & \frac{\sqrt{3}}{2} & -\frac{\sqrt{3}}{2} \\ \frac{1}{2} & \frac{1}{2} & \frac{1}{2} \end{bmatrix} \begin{bmatrix} i_{l-a} \\ i_{l-b} \\ i_{l-c} \end{bmatrix} \quad (19)$$

By performing the Laplace conversion the STF splits the HC from the FC by the given in Eq. 20.

$$\begin{bmatrix} \dot{i}_{l-\alpha}(s) \\ \dot{i}_{l-\beta}(s) \end{bmatrix} = \frac{k_2}{s} \begin{bmatrix} i_{l-\alpha}(s) - i'_{l-\alpha}(s) \\ i_{l-\beta}(s) + i'_{l-\beta}(s) \end{bmatrix} + \frac{2\pi f_{c2}}{s} \begin{bmatrix} i'_{l-\beta}(s) \\ -i'_{l-\alpha}(s) \end{bmatrix} \quad (20)$$

Where, k_2 is the gain= 20 and f_{c2} is the cut-off-frequency = 50Hz system frequency. The HC in $\alpha - \beta - 0$ coordinates are obtained by Eq. 21.

$$\begin{aligned} i'_{l-\alpha} &= i_{l-\alpha} - i_{l-\alpha} \\ i'_{l-\beta} &= i_{l-\beta} - i_{l-\beta} \end{aligned} \quad (21)$$

$$\begin{aligned} i'_{l-d} &= i'_{l-\alpha} \sin(\omega t) - i'_{l-\alpha} \cos(\omega t) \\ i_{l-q} &= i_{l-\alpha} \cos(\omega t) + i_{l-\beta} \sin(\omega t) \end{aligned} \quad (22)$$

By the use of HC from Eq. 21 and SYP from Eq. 18, the HC in d-frame is obtained. The reference current generation and stable DC-Link voltage plays a vital role in determining the performance of the SUAPF. However, if load changes the active power flow in the SUAPF may vary which leads to voltage instable across DC-Link. So, in order to regulate the voltage across the DC link the active power in SUAPF is made equal to the switching losses. The suggested ANNISMHC injects an appropriate error current signal Δi_{dc} . The mathematical expression for the calculation of DC-Link voltage is given by Eq. 23.

$$\Delta i_{dc} = e_1(t) = V^{ref}_{dc} - V_{dc}(t) \quad (23)$$

The reference load current in d-axis can be calculated in Eq. 24.

$$i^{ref}_{l-d} = i'_{l-d} - \Delta i_{dc} \quad (24)$$

The $d - q$ reference load currents are transformed into $\alpha - \beta$ domain by applying Eq. 25. Later, the reference shunt injected currents are transformed into abc domain by Eq. 26.

$$\begin{bmatrix} i^{ref}_{l-\alpha} \\ i^{ref}_{l-\beta} \end{bmatrix} = \begin{bmatrix} \sin(\omega t) & \cos(\omega t) \\ -\cos(\omega t) & \sin(\omega t) \end{bmatrix} \begin{bmatrix} i^{ref}_{l-d} \\ i^{ref}_{l-q} \end{bmatrix} \quad (25)$$

$$\begin{bmatrix} i^{ref}_{sh-a} \\ i^{ref}_{sh-b} \\ i^{ref}_{sh-c} \end{bmatrix} = \sqrt{\frac{2}{3}} \begin{bmatrix} 1 & 0 \\ -\frac{1}{2} & \frac{\sqrt{3}}{2} \\ -\frac{1}{2} & -\frac{\sqrt{3}}{2} \end{bmatrix} \begin{bmatrix} i^{ref}_{l-\alpha} \\ i^{ref}_{l-\beta} \end{bmatrix} \quad (26)$$

The errors currents obtained from the comparison of the actual and reference signals are transferred to a hysteresis control in order to produce appropriate gating pulses.

3.3.1 Proposed ANNISMHC

ANN is one among the famous Artificial intelligence technique which is a human-inspired mathematical model and very adaptable for the application to power electronic system control. MLPs are the familiar neural networks. The advantage of ANN consists of self learning ability, fault tolerance and fast convergence and robustness etc. Architecture of ANN consists 3 layers which are IL, HL, and OL. The most significant factor that affects the performance of ANN is the learning algorithm selected for training. Training is a process of searching for the best group of

weights that links the neurons of the ANN between the layers to reduce the error.

In MLP networks, neurons between the layers are interrelated by numerical weights, and each neuron consists of summation and activation functions. The purpose of summation function is to sum up the product of inputs and weights, and bias as shown in Eq. (27) where w_{pk} is the connection weight connecting I_p to neuron k , β_k is a bias term and m is the total number of neuron inputs. Usually, a nonlinear activation function like sigmoid function is used given in Eq. (28). Therefore, the output of the neuron k can be described as in Eq. (29).

$$S_k = \sum_{p=1}^m w_{pk} I_p + \beta_k \quad (27)$$

$$f(x) = \frac{1}{1 + e^{-x}} \quad (28)$$

$$O_k = f_k \left(\sum_{p=1}^m w_{pk} I_p + \beta_k \right) \quad (29)$$

MSE is evaluated by Eq. (30) where, O is the actual output, \bar{O} is the forecasted one, and n is the total instances.

$$MSE = \frac{1}{n} \sum_{p=1}^m (O_p - \bar{O}_p)^2 \quad (30)$$

In the proposed work single layer feed- forward back propagation ANN is trained for DC-Link balancing V_{dc}^{ref} is compared with V_{dc} and its error is taken as the input data while the desired output Δi_{dc} is given as the target data to the ANN. Fig 5 shows the ANN structure for DC-Link with 100 neurons in HL and Fig. 6 shows architecture of ANNC for DC-Link. It was proved [32] that MLP with single hidden layer is adequate to approximate any function.

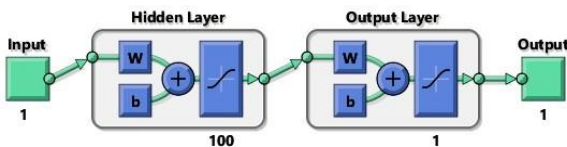


Fig. 5. Structure of ANNC for DC-link

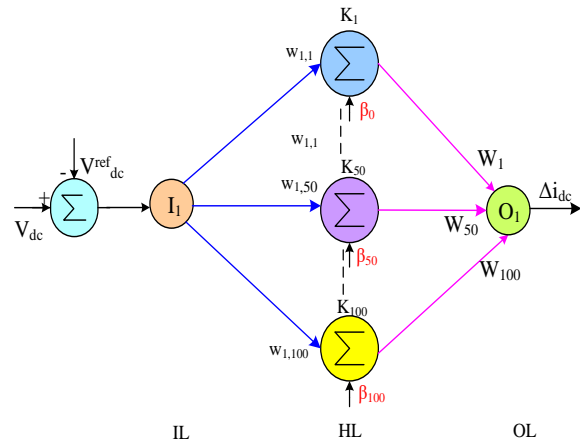


Fig.6. Architecture of ANNC controller for DC-Link

The Pseudo code for the proposed feed forward back propagation is outlined below:

Input: Problem size, patterns, max number of iterations, learning rate

Output: Network

Network \leftarrow construct Network layer ();

Network weight \leftarrow Initialize weights (Network, Problem size);

for $i=1$ to maximum iteration do,

Pattern _{i} \leftarrow select input pattern;

Output _{i} \leftarrow forward propagate (patterns, Network);

Back propagate error:

Update weights (patterns, output, network, learning rate);

End

Return network;

SMC is a non-linear controller generally used to control non-linear behavior power electronic FACTS devices the major role of SMC is the surface specification, generally called as a sliding-surface. The prime feature is to regulate the system within its surface. The main steps involved in SMC controllers are highlighted below 1) sliding-surface suggestion, 2) identification of presence of SM surface, and 3) stability analyses of the surface.

The error $e(n)$ is evaluated by Eq. (31).

$$x_1 = V_{dc}^{ref} - V_{dc} = e(n) \quad (31)$$

The derivative of the calculated error is obtained by Eq. (32).

$$x_2 = \frac{1}{T} e(n) - e(n-1) \quad (32)$$

Where, T is interval of time, and x_1 and x_2 are state space variables whose equation is given by Eq. (33)

$$\dot{x} = \begin{bmatrix} \dot{x}_1 \\ \dot{x}_2 \end{bmatrix} = \begin{bmatrix} 0 & 1 \\ 0 & 0 \end{bmatrix} \begin{bmatrix} x_1 \\ x_2 \end{bmatrix} + \begin{bmatrix} 0 \\ -k \end{bmatrix} \mu \quad (33)$$

The state space equation of sliding plane is represented by Eq. (34) and (35) respectively.

$$s = [C \quad 1] \begin{bmatrix} x_1 \\ x_2 \end{bmatrix} = Cx_1 + x_2 \quad (34)$$

$$\dot{s} = [C \quad 1] \begin{bmatrix} \dot{x}_1 \\ \dot{x}_2 \end{bmatrix} = C\dot{x}_1 + \dot{x}_2 \quad (35)$$

Power rate reaching law is given as,

$$\dot{s} = -L|s|^\alpha \text{sgn}(s) \quad (36)$$

Where,

$$\text{sgn}(s) = \begin{cases} 1 & \text{for } s > 0 \\ -1 & \text{for } s < 0 \end{cases} \quad (37)$$

The control law μ is calculated from Eqs. (38)

$$\mu = \frac{1}{K} [Cx_2 + L|s|^\alpha \text{sgn}(s)] \quad (38)$$

The control action is incorporated to get the modified control-law as given in Eq. (39).

$$\mu = \frac{1}{K} [Cx_2 + L|s|^\alpha \text{sgn}(s)] + K_i * \int_0^t e(\tau) d\tau \quad (39)$$

3.4 Series Controller

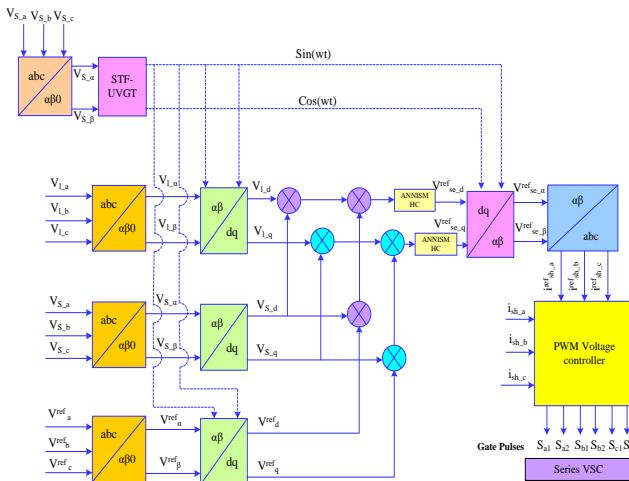


Fig.7. series controller

The main purpose of SEAPF is to eliminate voltage related PQ issues by injecting appropriate voltage through interfacing transformer. By using Eq.40 supply voltages are shifted into $\alpha - \beta - 0$ frame.

$$\begin{bmatrix} V_{S-\alpha} \\ V_{S-\beta} \\ V_{S-0} \end{bmatrix} = \sqrt{\frac{2}{3}} \begin{bmatrix} 1 & -\frac{1}{2} & -\frac{1}{2} \\ 0 & \frac{\sqrt{3}}{2} & -\frac{\sqrt{3}}{2} \\ \frac{1}{2} & \frac{1}{2} & \frac{1}{2} \end{bmatrix} \begin{bmatrix} V_{S-a} \\ V_{S-b} \\ V_{S-c} \end{bmatrix} \quad (40)$$

$$\begin{bmatrix} V_{S-d} \\ V_{S-q} \end{bmatrix} = \begin{bmatrix} \cos(\omega t) & \sin(\omega t) \\ -\sin(\omega t) & \cos(\omega t) \end{bmatrix} \begin{bmatrix} V_{S-\alpha} \\ V_{S-\beta} \end{bmatrix} \quad (41)$$

The 3ω voltage is transformed into $d - q$ two phase using park conversion by using Eq. 41.

$$\begin{bmatrix} V_{l-\alpha} \\ V_{l-\beta} \\ V_{l-0} \end{bmatrix} = \sqrt{\frac{2}{3}} \begin{bmatrix} 1 & -\frac{1}{2} & -\frac{1}{2} \\ 0 & \frac{\sqrt{3}}{2} & -\frac{\sqrt{3}}{2} \\ \frac{1}{2} & \frac{1}{2} & \frac{1}{2} \end{bmatrix} \begin{bmatrix} V_{l-a} \\ V_{l-b} \\ V_{l-c} \end{bmatrix} \quad (42)$$

$$\begin{bmatrix} V_{l-d} \\ V_{l-q} \end{bmatrix} = \begin{bmatrix} \cos(\omega t) & \sin(\omega t) \\ -\sin(\omega t) & \cos(\omega t) \end{bmatrix} \begin{bmatrix} V_{l-\alpha} \\ V_{l-\beta} \end{bmatrix} \quad (43)$$

By applying Eq.42 the load voltages are shifted into $\alpha - \beta - 0$ frame and to two phase $d - q$ domain by Eq. 46 by applying clark and park transformations.

$$\begin{bmatrix} V^{ref}_a \\ V^{ref}_b \\ V^{ref}_c \end{bmatrix} = V_{max} \begin{bmatrix} \sin(\omega t) \\ \sin(\omega t - 2\pi/3) \\ \sin(\omega t + 2\pi/3) \end{bmatrix} \quad (44)$$

$$\begin{bmatrix} V^{ref}_\alpha \\ V^{ref}_\beta \\ V^{ref}_0 \end{bmatrix} = \sqrt{\frac{2}{3}} \begin{bmatrix} 1 & -\frac{1}{2} & -\frac{1}{2} \\ 0 & \frac{\sqrt{3}}{2} & -\frac{\sqrt{3}}{2} \\ \frac{1}{2} & \frac{1}{2} & \frac{1}{2} \end{bmatrix} \begin{bmatrix} V^{ref}_a \\ V^{ref}_b \\ V^{ref}_c \end{bmatrix} \quad (45)$$

$$\begin{bmatrix} V^{ref}_d \\ V^{ref}_q \end{bmatrix} = \begin{bmatrix} \cos(\omega t) & \sin(\omega t) \\ -\sin(\omega t) & \cos(\omega t) \end{bmatrix} \begin{bmatrix} V^{ref}_\alpha \\ V^{ref}_\beta \end{bmatrix} \quad (46)$$

Similarly, reference voltage signal is calculated in abc by following Eq. 44 by applying STF-UVGM to obtain maximum peak voltage value V_{max} from the fundamental component. The load voltages are transformed into $\alpha - \beta - 0$ coordinates and to two phase $d - q$ domain by Eq. 45-46 by applying clark and park transformations.

$$\begin{aligned} V^{ref}_{se-d} &= (V^{ref}_d - V_{S-d}) - (V_{l-d} - V_{S-d}) \\ V^{ref}_{se-q} &= (V^{ref}_q - V_{S-q}) - (V_{l-q} - V_{S-q}) \end{aligned} \quad (47)$$

$$\begin{bmatrix} V_{se_a} \\ V_{se_b} \end{bmatrix} = \begin{bmatrix} \sin(\omega t) & \cos(\omega t) \\ -\cos(\omega t) & \sin(\omega t) \end{bmatrix} \begin{bmatrix} V_{se_d}^{ref} \\ V_{se_q}^{ref} \end{bmatrix} \quad (48)$$

$$\begin{bmatrix} V_{se_a}^{ref} \\ V_{se_b}^{ref} \\ V_{se_c}^{ref} \end{bmatrix} = \sqrt{\frac{2}{3}} \begin{bmatrix} 1 & 0 \\ -\frac{1}{2} & \frac{\sqrt{3}}{2} \\ -\frac{1}{2} & -\frac{\sqrt{3}}{2} \end{bmatrix} \begin{bmatrix} V_{se_a}^{ref} \\ V_{se_b}^{ref} \end{bmatrix} \quad (49)$$

The reference series injected voltage obtained from the difference between the actual reference source and load voltage demonstrated in Eq. 47-49. The injected series voltage passes through the PWM controller to produce the pulses for SEAPF given in Fig.7.

4. Simulation and Results

To analyze the performance efficiency of the suggested controller of U-SPBS a 3 ϕ distribution system was selected. The proposed system's simulink model was created in Matlab version 2016 with solar system is given in Fig. 8 (a) & (b) respectively. Five test studies with multiple combinations of balanced/ unbalance/ non-linear loads, supply voltages, variable irradiation and conditions like swell/sag/disturbance with constant temperature of 25⁰c was considered to attest the extraordinary performance of ANNISMHC on proposed U-SPBS as shown in Table 4.

The V_s was considered to be balanced for case studies 1, 2 and un-balanced for 3, 4 and 5 respectively with various combinations of swell/ sag, disturbance voltages with variable irradiation and constant temperature conditions. In addition, the THD was obtained for i_s of the proposed system for all the case studies and further it is compared with those of PIC, SMC and FLC as illustrated in Fig.9 by Eq. 50. The PF is obtained from the THD by applying Eq. 50 for all considered case studies as given in Fig.10. The U-SPBS and load specifications are exhibited in Table-3.

$$THD = \frac{\sqrt{\sum_{n=2}^{\alpha} V_{n_rms}^2}}{V_{f_rms}} \quad (50)$$

Where, V_{n_rms} is the RMS voltage of the nth harmonic and V_{f_rms} is the RMS voltage of fundamental component.

$$PF = \cos \theta * \frac{1}{\sqrt{1+THD^2}} \quad (51)$$

Here, θ is the measured angle between voltage and current, while $\frac{1}{\sqrt{1+THD^2}}$ represents displacement factor.

The source voltage sag and, swell ($V_{sag/swell}$) is evaluated by Eq. (52)

$$V_{sag/swell} = \frac{V_l - V_s}{V_l} = \frac{V_{se}}{V_l} \quad (52)$$

The series compensated voltage of U-SPBS is calculated by Eq. (53)

$$V_{se} = V_l - V_s \quad (53)$$

The shunt compensated current is specified by Eq. (54)

$$i_{sh} = i_i - i_s \quad (54)$$

Table 3: Ratings of U-SPBS

Source	$V_s : 415V ; f : 50Hz R_s : 0.1 \Omega ;$ $L_s : 0.151 mH$
SEAPF	$R_{se} : 1 \Omega ; L_{se} : 3.60 mH ; C_{se} : 60.0 \mu f$
SUAPF	$R_{sh} : 0.00101 \Omega ; L_{sh} : 2.150 mh ;$ $C_{sh} : 1.0 \mu F$ Hysteresisband: 0.01 A
DC link	$C_{dc} : 9400 \mu f ; V_{dc} : 700 V$

In case1, the supply voltage was considered to be balanced and sagged by 30% during the interval of 0.20-0.30 sec and swelled by 30% during 0.40-0.50 sec. In addition, disturbance was also introduced during the time period of 0.60-0.70 sec, as illustrated in Fig. 11(a). The waveform of load current was observed to be un-sinusoidal and balanced because of nonlinear balanced load is illustrated in Fig. 11(b). However, it clearly exhibits that the U-SPBS can eliminate voltage related and current related PQ issues successfully through appropriate compensation. Such improvement in the shapes of waveforms also reciprocated in the THD and power factor values. Therefore, the current THD was decreased from 20.54% to 2.44%, which is smaller when compared to those of other methods as given in Fig. 9 and the PF enhances from 0.7144 to 0.9989 by supplying the required voltages and currents. In addition, the suggested controller provides a constant voltage across the DC link during 1000W/m² irradiation and constant temperature of 25⁰c as shown in Fig. 11(c).

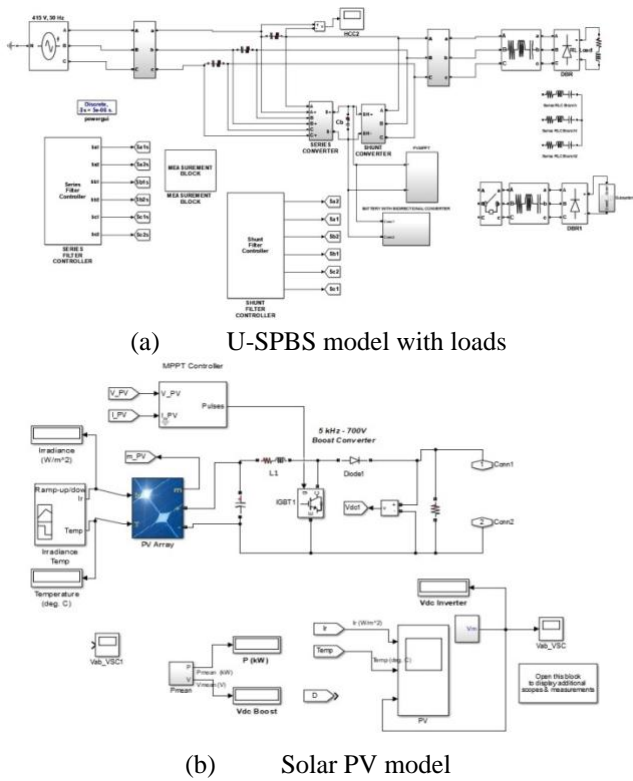


Fig.8. Matlab/ simulink model

In case2, the supply voltage was considered to be balanced with the voltage related issues as similar to the case1, but irradiation of 800W/m² as exhibited in Fig. 12(a). Here, the load current waveform was observed to be non sinusoidal and un-balanced due the non-linear balanced and unbalanced loads acting simultaneously as given in Fig. 12(b). It is clearly visible from the waveforms that the U-SPBS was able to voltage related PQ problems effectively and diminishes THD from 15.31% to 2.67% thus enhancing the PF from 0.8552 to 0.9989 by injecting compensating voltages and currents. However, as demonstrated in Fig. 12(b) suggested controller works efficiently in maintaining constant voltage across DC-Link during load and irradiation variation simultaneously.

In case3, the source voltage was considered to be unbalanced for 3øbalanced rectifier load with 1000W/m² irradiation as given in Fig. 13(a). The load current was observed to be highly non-sinusoidal and balanced as in Fig. 13(b). However, the ANNISMHC was able to suppress the THD from 12.63% to 3.42%, improves PF from 0.7399 to 0.9988 and balances load voltage successfully by injecting suitable appropriate currents and voltages. In addition, it also stables DC-Link voltage as in Fig. 13(c).

Table 4: Test cases considered under constant 25⁰c temperature

Condition / Load	Case-1	Case-2	Case-3	Case-4	Case-5
Balanced Supply voltage	✓	✓			

Unbalanced Supply voltage			✓	✓	✓
Voltage swell, sag and disturbance	✓	✓			
Steady state current	✓	✓	✓	✓	✓
Steady state voltage			✓	✓	✓
Irradiation 1000W/m ²	✓		✓		✓
Irradiation 800W/m ²		✓		✓	
Load1: Balanced-Rectifier-30.00Ω & 20.00mH	✓	✓			✓
Load2: Unbalanced R-L-				✓	
R: 10, 20 & 15 ohm; L: 9.50 mH, 10.50 mH & 18.50 mH.		✓			
Load3: Induction-Furnace- LC = 400mh, 50μF					✓
RL = 10ohm,100mH					

In case4, the supply voltage and load both was considered to be unbalanced with 800W/ m² given in Fig. 14(a). The load current waveforms are observed to be sinusoidal but unbalanced as shown in Fig. 14(b). The ANNISMHC is able to suppress the harmonics in the current waveform and decreases THD from 19.63% to 4.17% while boosting up the PF from 0.6382 to 0.9998. Fig.14 (c) exhibits its performance in regulating DC-Link voltage during load variation.

Controller	Case1	Case2	Case3	Case4	Case5
Without SH-SPVBS	20.54	15.71	12.63	19.63	26.12
PIC	4.97	5.08	4.25	5.02	5.23
SMC	4.74	3.24	4.23	4.09	4.26
FLC	4.01	3.13	3.14	4.14	4.17
PIC [20]	3.28	--	--	--	--
SMC [20]	2.44	--	--	--	--
PIC [25]	14.74	--	--	--	--
FLC [25]	6.13	--	--	--	--
PIC [27]	3.65	--	--	--	--
FLC [27]	2.52	--	--	--	--
ANNISMHC	2.44	2.67	3.42	4.17	3.43

Table 5 % THD comparison

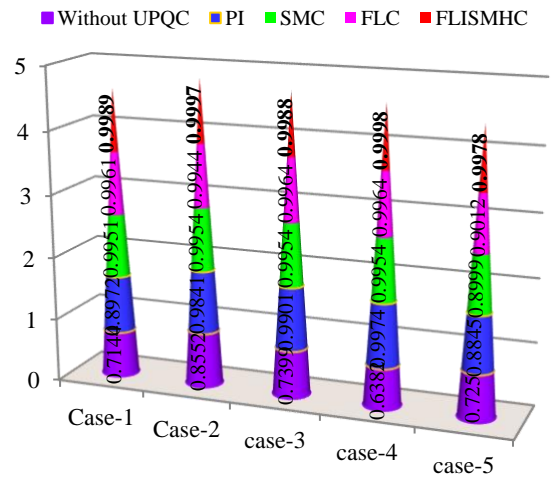


Fig.10. PF for test cases

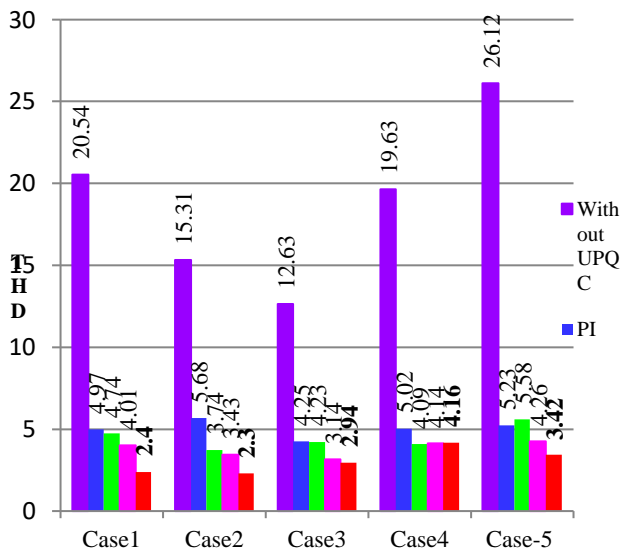
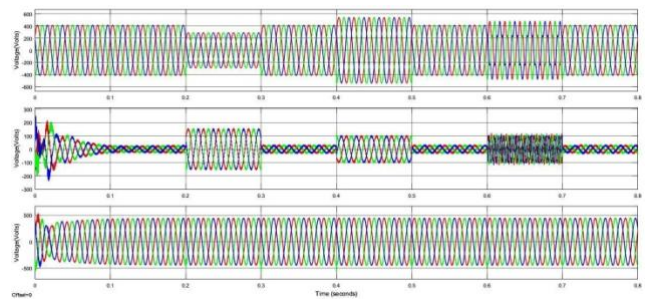
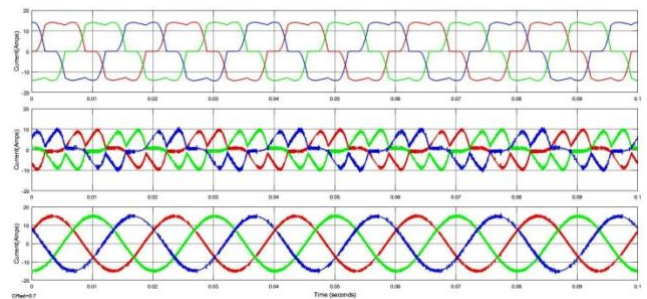


Fig.9. THD comparison bar chat

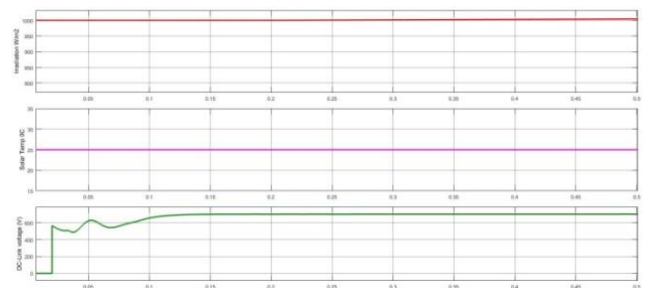
In case5- the unbalanced supply voltage was considered with the combination of 3ω rectifier load and induction furnace loads with 1000W/m² irradiation as illustrated in Fig. 15(a). The load current was balanced with non-sinusoidal structure as in Fig. 15(b). The suggested ANNISMHC diminishes the THD from 26.12% to 3.43% and boosts up PF from 0.725 to 0.9978 effectively. The THD for all the proposed test studies is as given in Fig.17. The stable DC-link voltage was maintained as shown in Fig.16 during the dynamic variation in solar irradiation under constant temperature. To show the superior performance the proposed controller is compared with the controllers that are available in the literature is given in table 5.



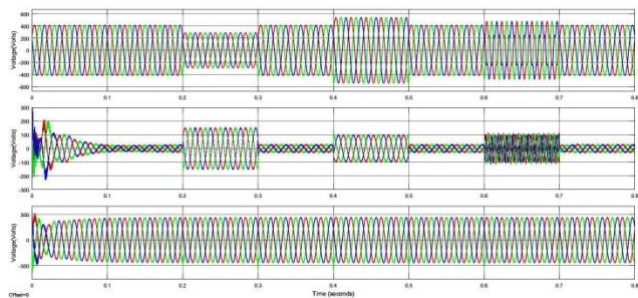
(a) V_s, V_{se}, V_l



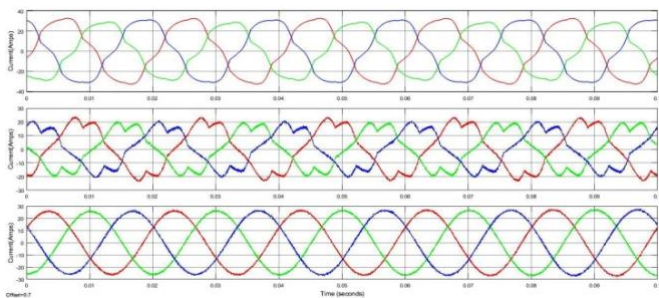
(b) i_l, i_{sh}, i_s



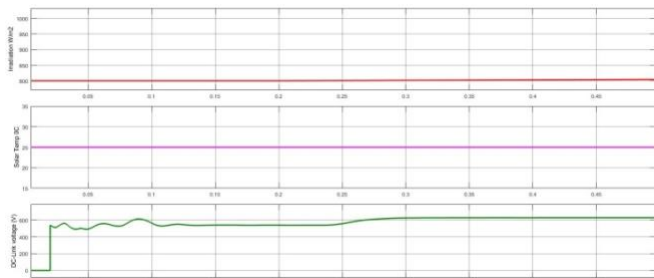
(C) Solar irradiation, temperature, DC-link voltage
Fig.11. Waveforms of U-SPBS for case-1



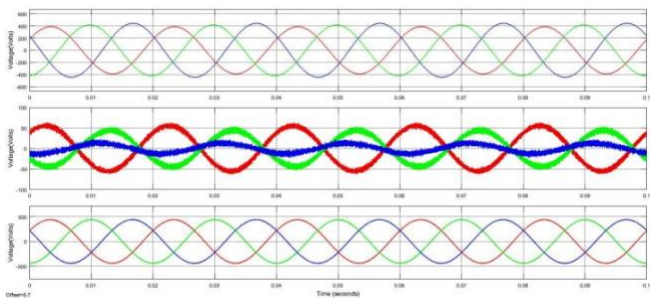
(a) V_S, V_{se}, V_l



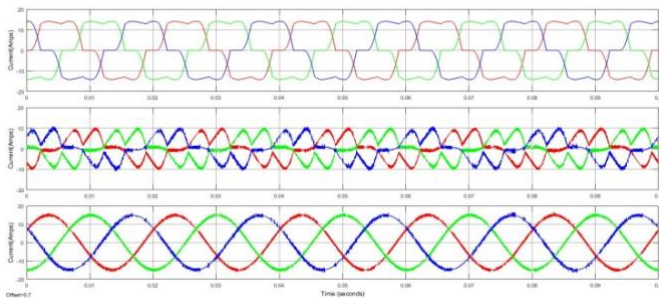
(b) i_l, i_{sh}, i_S



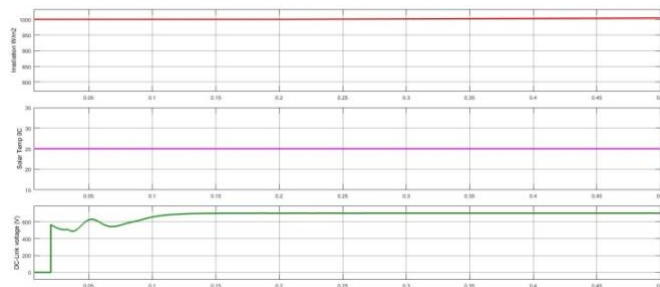
(c) Solar irradiation, temperature, DC-link voltage
Fig.12. Waveforms of U-SPBS for case-2



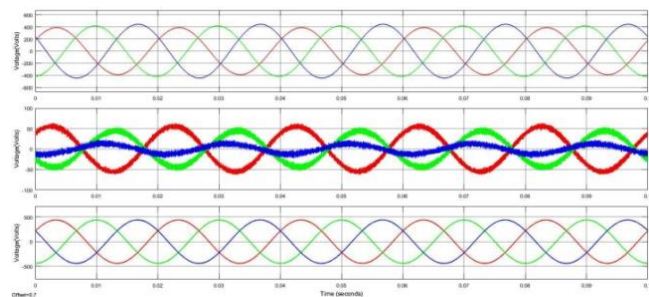
(a) V_S, V_{se}, V_l



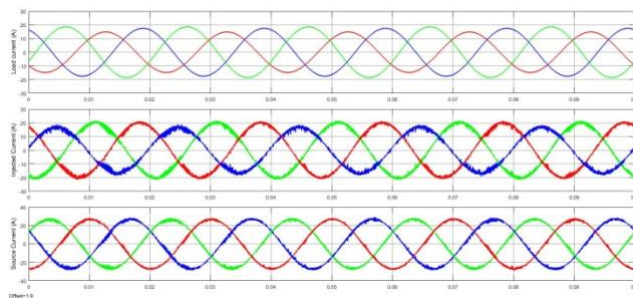
(b) i_l, i_{sh}, i_S



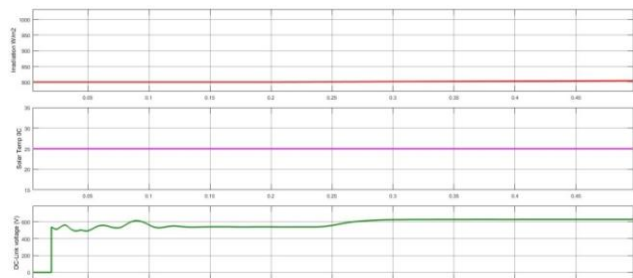
(c) Solar irradiation, temperature, DC-link voltage
Fig.13. Waveforms of U-SPBS for case-3



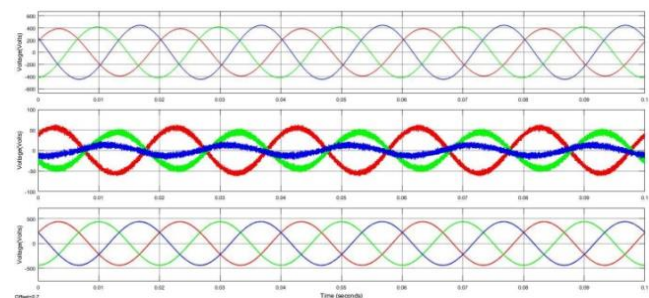
(a) V_S, V_{se}, V_l



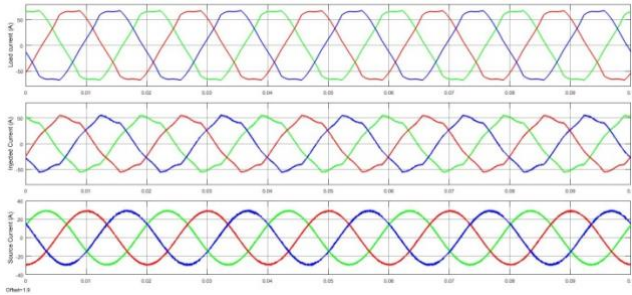
(b) i_l, i_{sh}, i_S



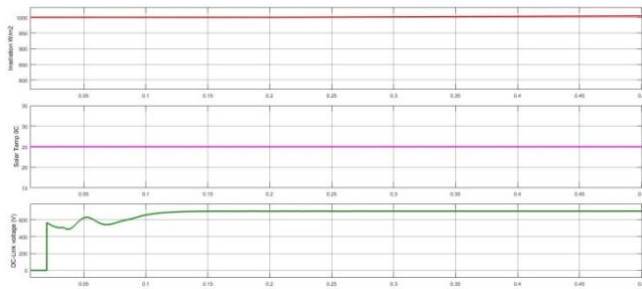
(c) Solar irradiation, temperature, DC-link voltage
Fig.14. Waveforms of U-SPBS for case-4



(a) V_S, V_{se}, V_l



(b) i_l, i_{sh}, i_s



(c) Solar irradiation, temperature, DC-link voltage
Fig.15. Waveforms of U-SPBS for case-5

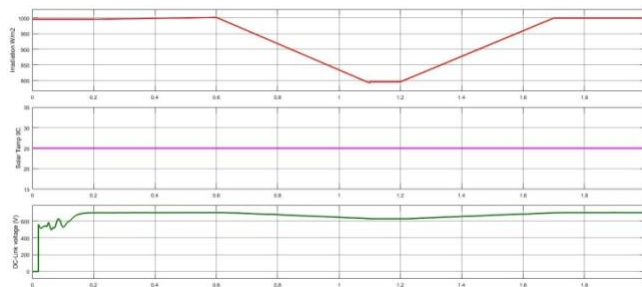
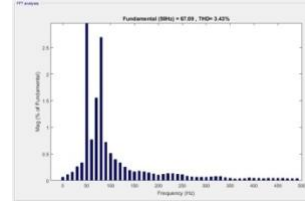
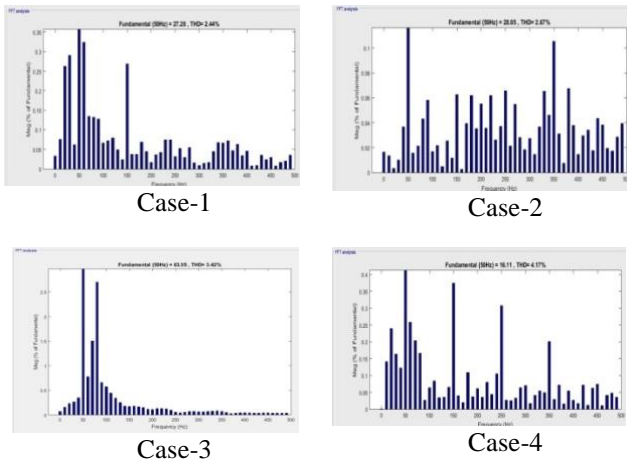


Fig.16. Waveforms for U-SPBS during (a) solar irradiation variation (b) 25⁰c constant temperature (c) DC-Link voltage with settling time



Case-5

Fig.17. THD spectrum for case studies

5. Conclusion

The hybrid controller with the combination of ANNC and ISMC properties are proposed for STF based U-SPBS. The design of controllers for SPV and BS were also specified in addition to the development of ANNISMHC for shunt controller with an aim of quick stabilizing the DC-Link capacitance voltage, eliminating swell, sag, disturbances in supply voltage, suppressing the harmonics in current, and enhancing the PF. From the analysis on five cases it is clearly exhibited that the ANNISMHC was able to reduce the THDs within the limits of IEEE standards and PF to almost unity. Moreover, by the comparative analysis it has been proved that the performance was much better than controllers like PIC, SMC and FLC. The ANNISMHC also maintains the stable voltage across DC link. The proposed system can be further studied with Multi-level UPQC for micro-grid in distribution network as future work.

References

1. G. Vijayakumar, N. Gupta and R. A. Gupta, "Mitigation of power quality problems using shunt active power filters: A comprehensive review" 12th IEEE Conference on Industrial Electronics and Applications (ICIEA), 18-20 June 2017.
2. M. Kesler, and E. Ozdemir, "Synchronous-Reference-Frame-Based Control Method for UPQC under Unbalanced and Distorted Load Conditions", IEEE Transactions on Industrial Electronics, Vol. 58, No. 9, pp. 3967-3975, September 2011.
3. M. Suresh, and A. K. Panda, "PI and Fuzzy Logic Controller based 3-phase 4-wire Shunt active filter for mitigation of Current harmonics with Id-Iq Control Strategy", Journal of power Electronics, Vol. 11, No. 6, pp. 914-921, Nov 2011.
4. S R. Das, P. K. Ray, A. Mohanty and G. Panda, "Power Quality Enhancement in PV and Battery Storage Based Microgrid Using Hybrid Active Filter" 2020 3rd International Conference on Energy, Power and Environment: Towards Clean Energy Technologies, 5-7 March 2021.
5. M. Suresh and A. K. Panda, "RTDS hardware implementation and simulation of SHAF for mitigation of harmonics using p-q control strategy with PI and Fuzzy logic controllers", Frontiers of Electrical and Electronic Engineering, Vol. 7, No. 4, pp. 427-437, Jun. 2012.

6. C.L. Hsiung, "Intelligent Neural Network-Based Fast Power System Harmonic Detection," *IEEE Transactions on Industrial Electronics*, Vol. 54, No. 1, pp. 43-52, Feb.2007.
7. P.K.Dash, S.K.Panda, T.H.Lee J.X.Xu and A.Rou tray, "Fuzzy and Neural Controllers for Dynamic Systems: an Overview". *IEEE*, May 1997.
8. S. Devassy, and B. Singh, "Design and Performance Analysis of Three-Phase Solar PV Integrated UPQC", *ICPS, IEEE-March 2016*.
9. V. K Krishna, S. K. Dash and K.R Geshma, "Development and Analysis of Power Quality by using Fuel cell based Shunt Active Power Filter", 2020 2nd International Conference on Innovative Mechanisms for Industry Applications (ICIMIA), 5-7 March 2020
10. K. Srilakshmi, C. N. Sujatha, P. K. Balachandran, L. Mihet-Popa, and N. U. Kumar, "Optimal Design of an Artificial Intelligence Controller for Solar-Battery Integrated UPQC in Three Phase Distribution Networks", *Sustainability*, Vol. 14, No. 21, Oct-2022.
11. K. Chandrasekaran, J. Selvaraj, C. R. Amaladoss and L. Veerapan, "Hybrid renewable energy based smart grid system for reactive power management and voltage profile enhancement using artificial neural network", *Energy Sources, Part A: Recovery, Utilization, and Environmental Effects*, Vol. 43, No. 19, pp. 2419–2442, March 2021.
12. K. Srilakshmi , N. Srinivas , P. K. Balachandran , J.G.P. Reddy, S. Gaddameedhi, N. Valluri, S. Selvarajan, "Design of Soccer League Optimization Based Hybrid Controller for Solar-Battery Integrated UPQC", *IEEE Access*, Vol. 10, pp. 107116-107136, Oct-2022.
13. Krishna Sarker, Debashis Chatterjee and S. K. Goswami, "A modified PV-wind-PEMFCS-based hybrid UPQC system with combined DVR/STATCOM operation by harmonic compensation", *International Journal of Modeling and Simulation*, Vol.41, No.4, pp. 243-255, March 2020.
14. T. S. Saggi, L. Singh, B. Gill and O. P. Malik, "Effectiveness of UPQC in Mitigating Harmonics Generated by an Induction Furnace", *Electrical power components and systems*, Taylor & Francis, Vol. 46, No. 6, pp. 629-636, Nov-2018.
15. S.S. Dheeban and N.B. Muthu Selvan, "ANFIS-based Power Quality Improvement by Photovoltaic Integrated UPQC at Distribution System", *IETE Journal of Research*, Feb-2021.
16. M. Ebadian, M. Talebi and R. Ghanizadeh, " A New Approach Based on Instantaneous Power Theory for Improving the Performance of UPQC Under Unbalanced and Distortional Load Conditions" , *Automatika, Journal for Control, Measurement, Electronics, Computing and Communications*, DOI: 10.7305/automatika.2015.07.750, Vol. 56, No. 2, pp. 226-237, Jan-2017.
17. M. Abdusalama, P. Poureb, S. Karimia and S. Saadateh, "New digital reference current generation for shunt active power filter under distorted voltage conditions", *Vol. 79*, pp. 759–765, Dec-2009.
18. M. Almelian. I. Mohd, M. Omran and U. Sheikh, "Performance of unified power quality conditioner (UPQC) based on fuzzy controller for attenuating of voltage and current harmonics", *IOP Conf. Series: Materials Science and Engineering*, 2018, 3, 012-084.
19. V. Vinothkumar, and R. Kanimozhi, "Power flow control and power quality analysis in power distribution system using UPQC based cascaded multi-level inverter with predictive phase dispersion modulation method", *Journal of Ambient Intelligence and Humanized Computing* **2021**, 12, 6445–6463.
20. S. Samal, and P.K. Hota, "Design and analysis of solar PV-fuel cell and wind energy based microgrid system for power quality improvement", *Cogent Engineering*, 2017, 4, 1-22.
21. S. Koganti, K. J. Koganti and S. R. Salkuti , Design of Multi-Objective-Based Artificial Intelligence Controller for Wind/Battery-Connected Shunt Active Power Filter, *Algorithms*, Vol. 15, No. 8, pp. 256, Aug-2022.
22. K. Srilakshmi, P. R. Babu, Y. Venkatesan, A. Palanivelu, Soccer league optimization for load flow analysis of power systems, , *International journal of numerical modelling electronic networks devices and fields* 35(2) (2022), 2709-2724.
23. A. Abdelnasser, A. H. Nafeh, A. El-Sehiemy Ragab, and A.A.S. Waleed, "Intelligent fuzzy-based controllers for voltage stability enhancement of AC-DC micro-grid with D-STATCOM", *Alexandria Engineering Journal* 2022, 61,2260-2293.
24. J. A. Sayed, R.A. Sabha and K.J. Ranjan, "Biogeography based optimization strategy for UPQC PI tuning on full order adaptive observer based control", *IET Generation, Transmission & Distribution* 2021, 15, 279-293.
25. U.K. Renduchintala, C. Pang, K. M. Tatikonda, L. Yang,"ANFIS-fuzzy logic based UPQC in interconnected microgrid distribution systems: Modeling, simulation and implementation", *The Journal of Engineering* 2021, 21, 1-29.
26. S. Devassy and B. Singh,"Performance analysis of solar pv array and battery integrated unified power quality conditioner for microgrid systems", *IEEE Transactions on Industrial Electronics*, 68(5) (2021), 4027 – 4035.
27. C. Pazhanimuthu, S. Ramesh," Grid integration of renewable energy sources (RES) for power quality improvement using adaptive fuzzy logic controller based series hybrid active power filter (SHAPF)", *Journal of Intelligent & Fuzzy Systems* 2018, 35, 749–766.
28. F. Ayadi; I. Colak; I. Garip, H. Bulbul, "Impacts of Renewable Energy Resources in Smart Grid", 8th International Conference on Smart Grid, Paris, pp. 183-188, June 2020.
29. I. Colak; R. Bayindir, S. Sagioglu, "The Effects of the Smart Grid System on the National Grids", 8th International Conference on Smart Grid, Paris, pp. 122-126, June 2020.
30. S. Jaber, A. M. Shakir, "Design and Simulation of a Boost-Microinverter for Optimized Photovoltaic System Performance", *International Journal of Smart Grid*, Vol. 5, No. 2, pp. 1-9, June 2021.

31. S. Ikeda, F. Kurokawa, "Isolated and wide input ranged boost full bridge DC-DC converter for improved resilience of renewable energy systems", San Diego, CA, USA, pp. 290-295, 5-8 Nov. 2017.
32. S. S. Dash, "Tutorial 1: Opportunities and challenges of integrating renewable energy sources in smart" 6th International Conference on Renewable Energy Research and Applications , San Diego, CA, USA, 5-8 Nov. 2017.
33. M. Tsai, C. Chu, W. Chen, "Implementation of a Serial AC/DC Converter with Modular Control Technology", 7th International Conference on Renewable Energy Research and Applications, Paris, France, pp. 245-250, Oct. 2018.
34. A. Thakallapelli, S. Ghosh; S. Kamalasan, "Real-time frequency based reduced order modeling of large power grid" IEEE Power and Energy Society General Meeting Boston, MA, USA, 17-21 July 2016.
35. A. Belkaid, I. Colak, K. Kayisli, R. Bayindir, Improving PV System Performance Using High Efficiency Fuzzy Logic Control, 8th International Conference on Smart Grid, Paris, pp.152-156, June 2020.